Supplemental Material

Reconciling coherent oscillation with rate modulation of irregular spiking activity in selective attention: gamma-range synchronization between sensory and executive cortical areas

Salva Ardid[1,2], Xiao-Jing Wang[2], David Gomez-Cabrero[1], and Albert Compte[1]

[1]Institut d'Investigacions Biomèdiques August Pi i Sunyer (IDIBAPS),

Villarroel 170, 08036 Barcelona, Spain

[2]Department of Neurobiology and Kavli Institute for Neuroscience,

Yale University School of Medicine, New Haven, CT

Index

Supplemental Figures

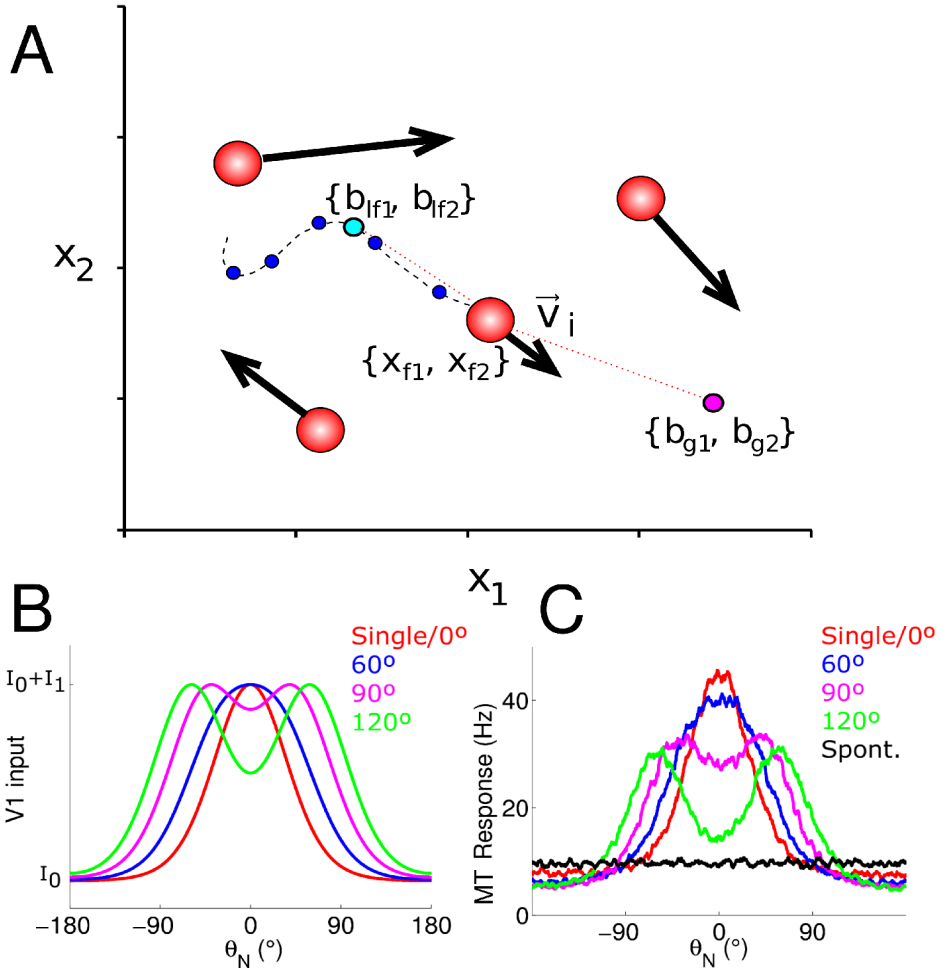

Supplemental Figure 1. Schematic representation of the particle swarm optimization algorithm used for finding network parameters that produce the required responses in area MT.

A, Schematic representation of the PSO algorithm (supplemental Methods, supplemental Eqs. 3 and 4) illustrating 4 particles in a 2-dimensional space for clarity (in our simulations, we had 50 particles in a 13-dimensional space). For one of the particles (center) a path with previously visited locations (dark blue dots) is drawn. The particle updates its velocity stochastically towards the location visited by this particle with best fitness value (cyan dot) and towards the best location found by the whole swarm (magenta dot). ***B,*** Injected V1 input to the MT model. This input takes into account maximal response normalization, thus the maximum activity in the network is conserved irrespective of whether a single moving or two transparent RDPs are present, or the separation between the two components during transparent motion. ***C,*** Characteristic population activity profiles for pyramidal cells in the MT model solutions. The background activity is near 10 Hz; peak of activity for a single RDP is around 45 Hz; there is slight suppression in this case in the

tails of the bell-shaped curve; and it implements mean activity normalization, so the mean activity remains unaltered for single moving RDP and for transparent motion, irrespective in this case of the separation between the two components.

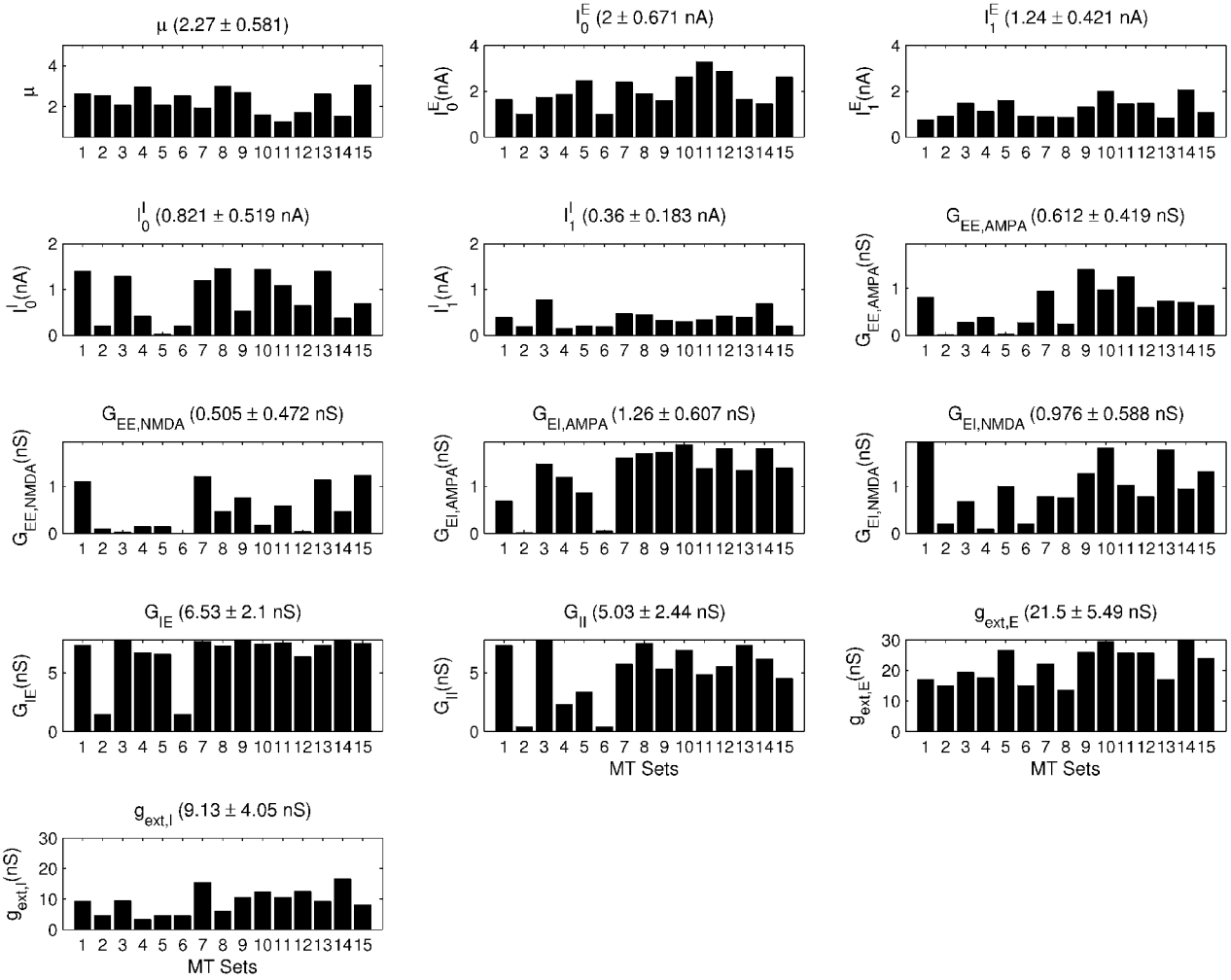

Supplemental Figure 2. Distribution of parameters in the MT network model solutions found by the optimization procedure.

Each panel shows the value of the corresponding parameter for each different MT network solution found with our optimization procedure. Those highly irregular parameter distributions point at the fact that we found MT networks very distinct with respect to their parameter values. The control model solution shown in the figures of the main text corresponds to the first model (first column in all panels). The second model solution corresponds to the MT model in (Ardid et al., 2007). Mean and standard deviation for each parameter are indicated in the title for each panel.

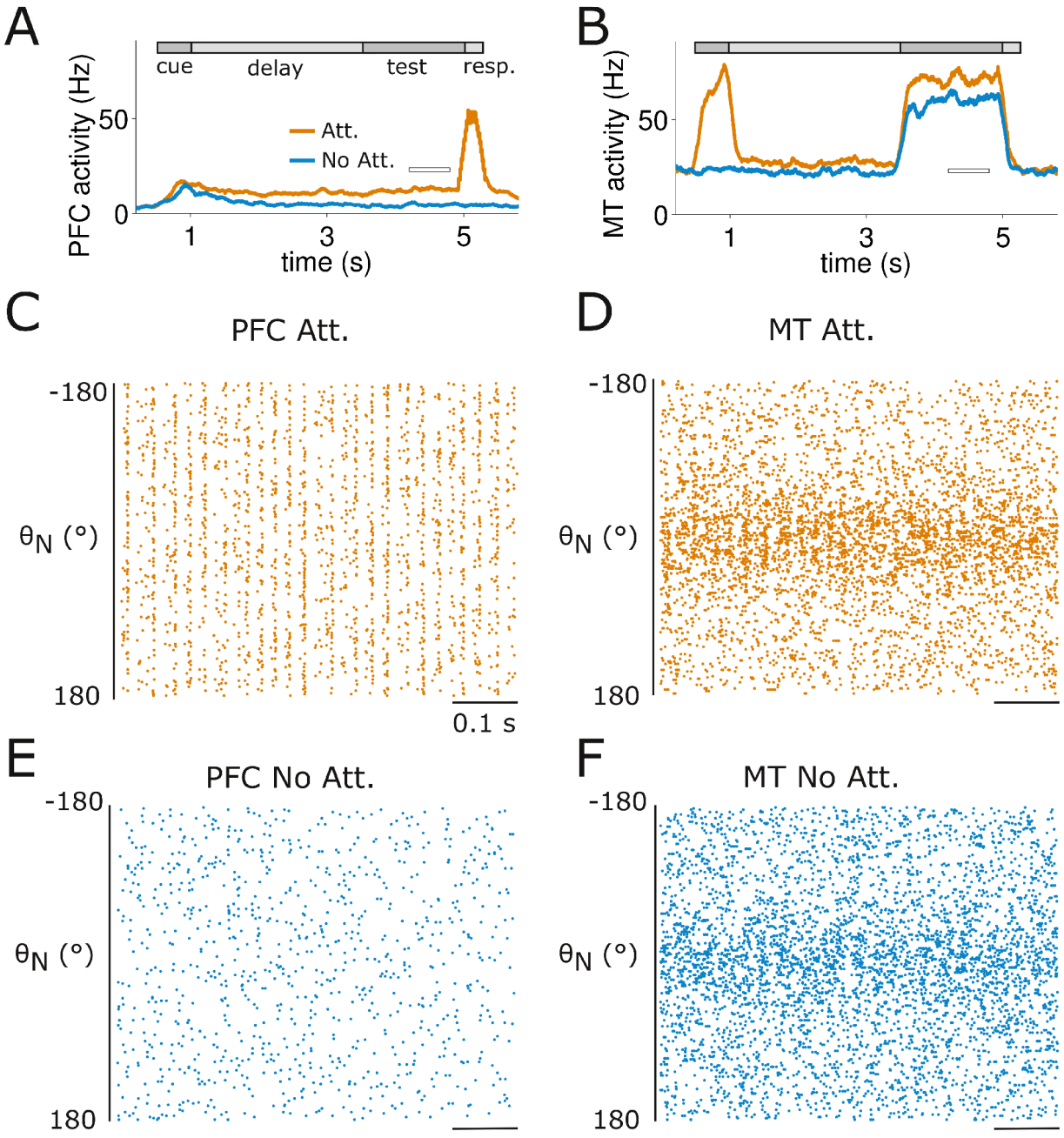

Supplemental Figure 3. Interneurons show similar patterns of spiking activity in the course of the attention task.

A, Average firing rate activity of one inhibitory neuron in the PFC network through the various task epochs and conditions (attention and no attention trials). Rates and dynamics are similar to excitatory neurons (Fig. 2*A*,*B*). ***B,*** Same for one inhibitory neuron in the MT network. ***C,*** Spatio-temporal graphs of spiking activity in small windows in the test epoch of attention trials for PFC inhibitory neurons show traces of synchronized activity. ***D,*** Same for MT inhibitory neurons. ***E,*** and ***F,*** Same in no-attention trials showing the lack of visually evident synchronization among the networks of interneurons.

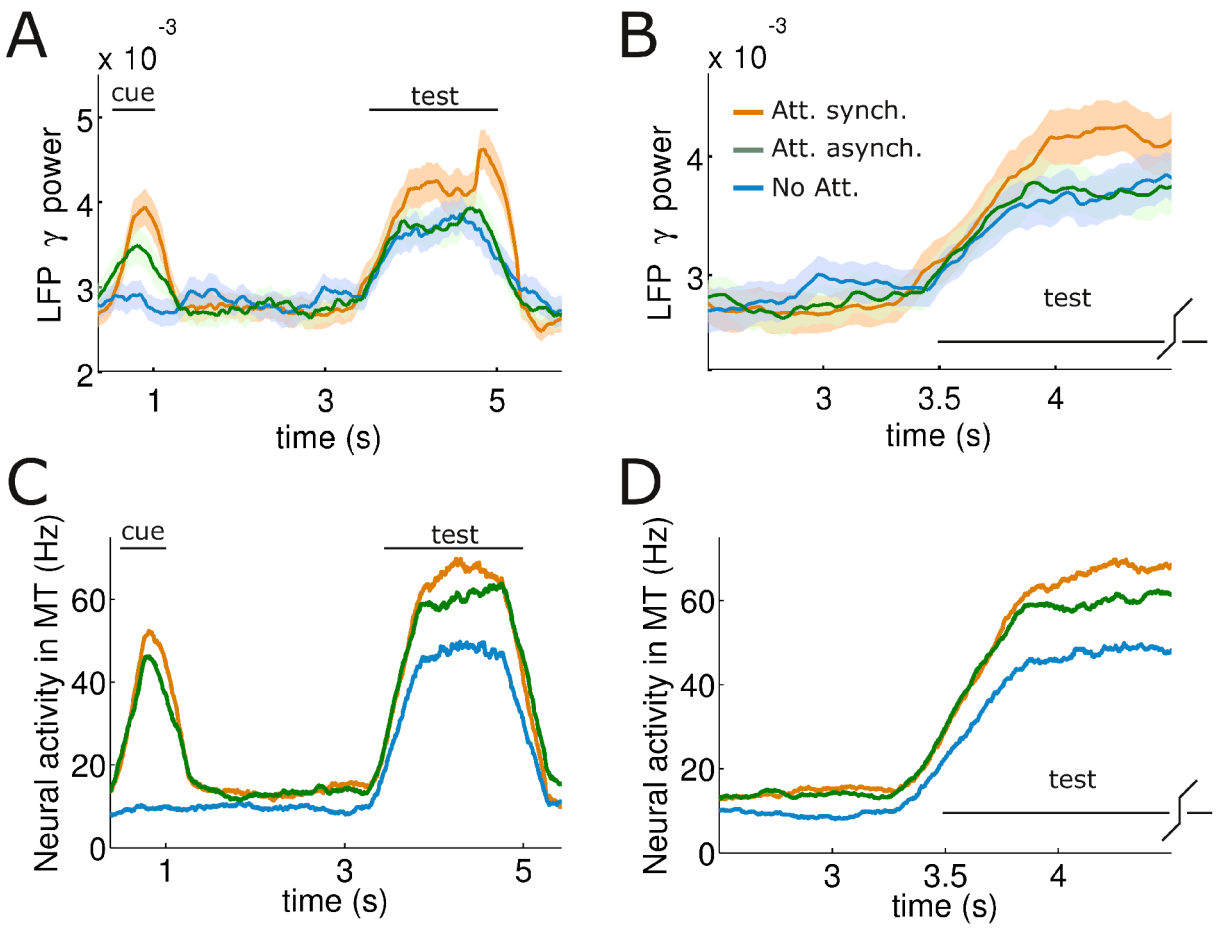

Supplemental Figure 4. The time course of LFP gamma power mimics rate modulations, but not for asynchronous top-down inputs.

A, Time resolved spectral power in the gamma band (30-50 Hz) of MT LFP in three different trials (synchronous attention, asynchronous attention and no attention) (N_t=70). ***B,*** zoom in of panel ***A*** around the time of test onset. ***C,*** Time histograms of spiking activity of an MT neuron in the three trials in ***A*** (N_t=20). ***D,*** zoom in of panel ***C*** around the time of test onset. The no-attention and synchronous-attention curves show similar time courses in ***A*** and ***C***, and in ***B*** and ***D***. However, the asynchronous-attention curve differs: In ***C*** and ***D*** it follows the synchronous-attention curve, whereas in ***A*** and ***B*** it follows the no attention curve. This shows that rate effects in the test period are only partially due to the enhancement of MT synchronization, and that the faster dynamics of activity onset in attention trials (panel ***D***) does not depend on enhanced synchronization in the MT local circuit.

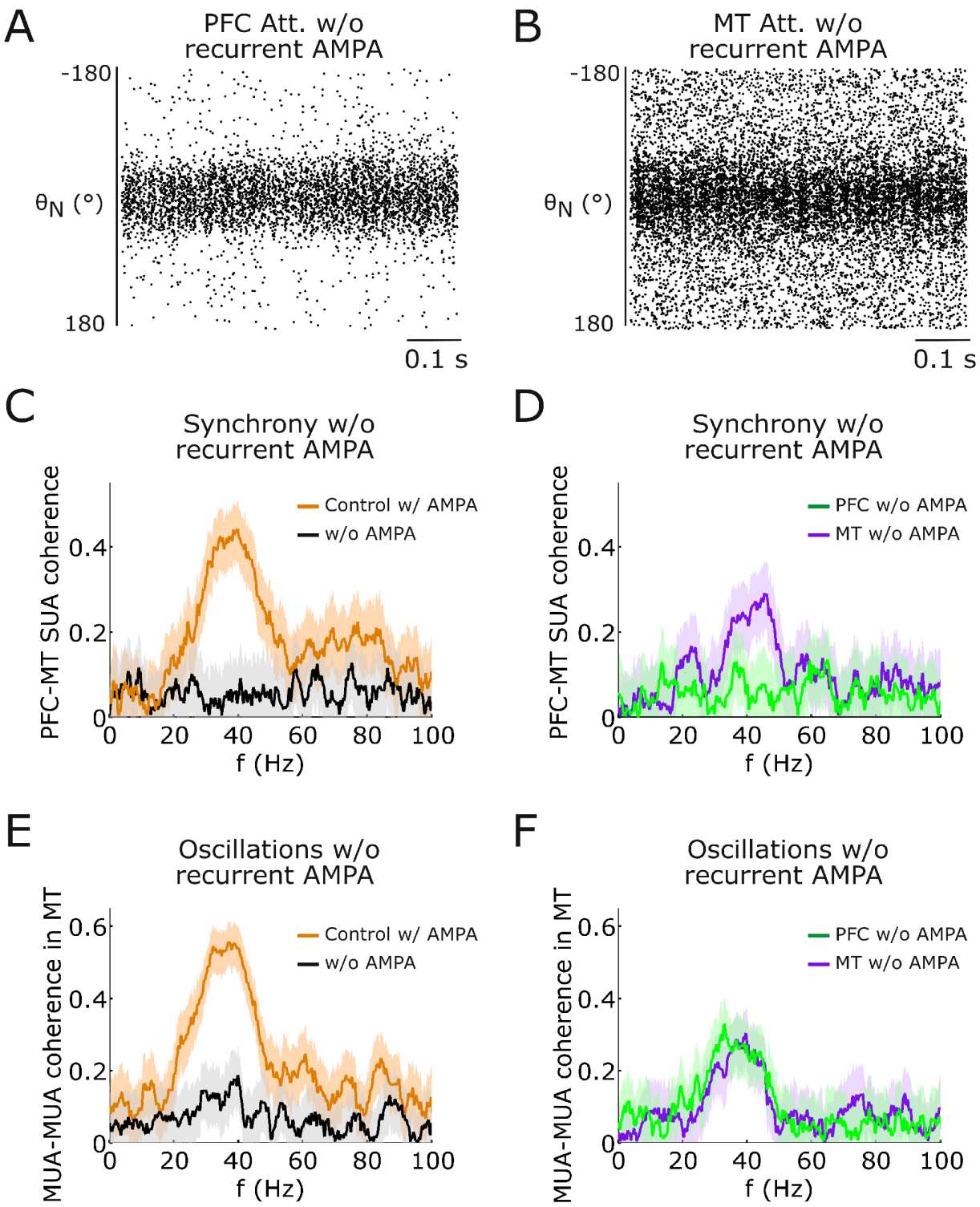

Supplemental Figure 5. Inter-areal synchronization and local oscillations in the gamma-range frequency are mediated by recurrent AMPA receptors.

Oscillations and synchrony in the model are based on the interplay between short time constants of recurrent AMPA synapses and medium time constants of recurrent $GABA_A$ synapses in each network. We show here that when we removed completely AMPA dynamics in the model compensating with NMDA synapses (PFC: $G_{EE,NMDA} = 0.830$ nS, $G_{EI,NMDA} = 0.654$ nS; MT: $G_{EE,NMDA} =$

1.50 nS, $G_{EI,NMDA}$ = 2.25 nS), then both inter-areal synchronization and local oscillations vanish. ***A,*** Spatio-temporal graph of test-period spiking activity in the PFC area network without recurrent AMPA shows the lack of oscillations in the WM circuit (Compare to Fig. 2*C*). ***B,*** Same for MT network (compare to Fig. 2*D*). In this case, remaining MT slight oscillations reflect oscillations coming from V1 sensory input. ***C,*** The gamma-range peak in the coherence between spike trains of one PFC neuron and one MT neuron (control in orange) disappears when there is no recurrent AMPA synapses in any of the circuits (black). ***D,*** Removing recurrent AMPA synapses of the PFC circuit completely abolishes inter-areal synchronization (green), while some significant coherence remains in the absence of AMPA recurrence in MT when AMPA-synapses mediate excitation in the PFC module (violet). ***E,*** The gamma-range peak in the coherence between pairs of MUA in MT (control in orange) disappears almost completely when there is no recurrent AMPA synapses in any of the circuits (black). ***F,*** Synchronization within MT is weaker, but is still significant, when AMPA receptors are removed in either one of the two networks.

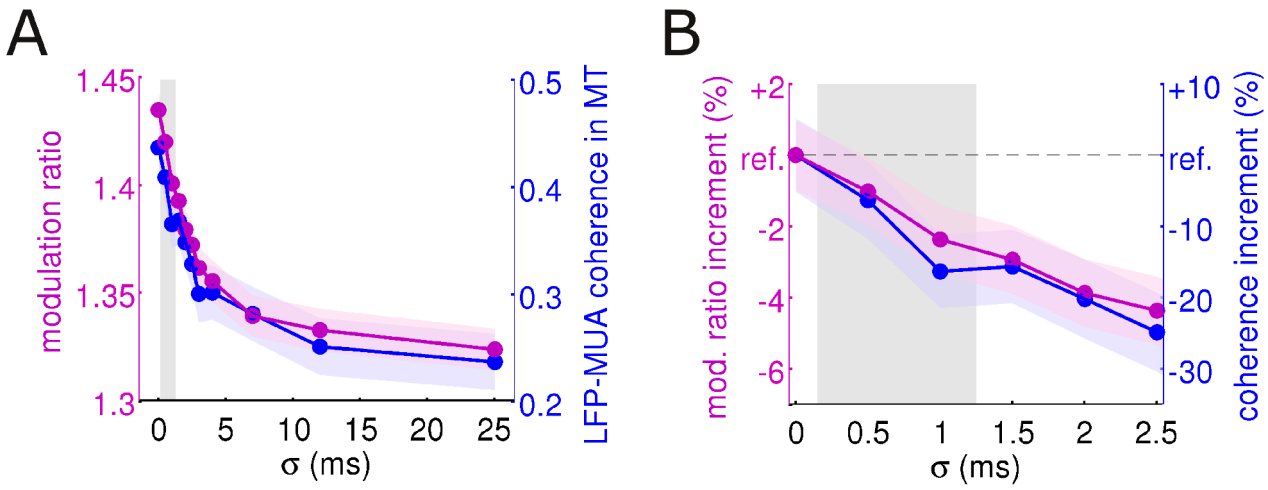

Supplemental Figure 6. Gamma-range synchrony in MT and modulation ratio of firing rates decrease with synaptic latency dispersion, but remain sizable for physiological values.

The exponential distribution from which conduction latencies for top-down synapses were randomly drawn was parametrically varied and the modulation ratio was computed as in Figure 7*B*. ***A,*** Parametric analysis of the dependence of the maximum value of modulation ratio (purple, see Fig. 7*B*) and MT LFP-MUA coherence (blue) with the s.d. of top-down (exponentially distributed) synaptic latencies σ. The reduction in inter-areal coherence mimicked the drop in peak modulation ratio as the standard deviation σ of top-down latencies increased, but remained high for physiologically plausible values (range 0.15-1.21 ms (Ghosh and Porter, 1988; Fanardjian and Papoyan, 1997; Sirota et al., 2005; Le Bé et al., 2007), gray shaded rectangle). ***B,*** Same as ***A*** but zooming in σ and computing changes relative to the control case σ=0. Physiological dispersion of synaptic latencies in long-range connections are therefore insufficient to eliminate the effect of inter-areal synchronization in the attentional modulations of firing rate responses in area MT (N_t=20).

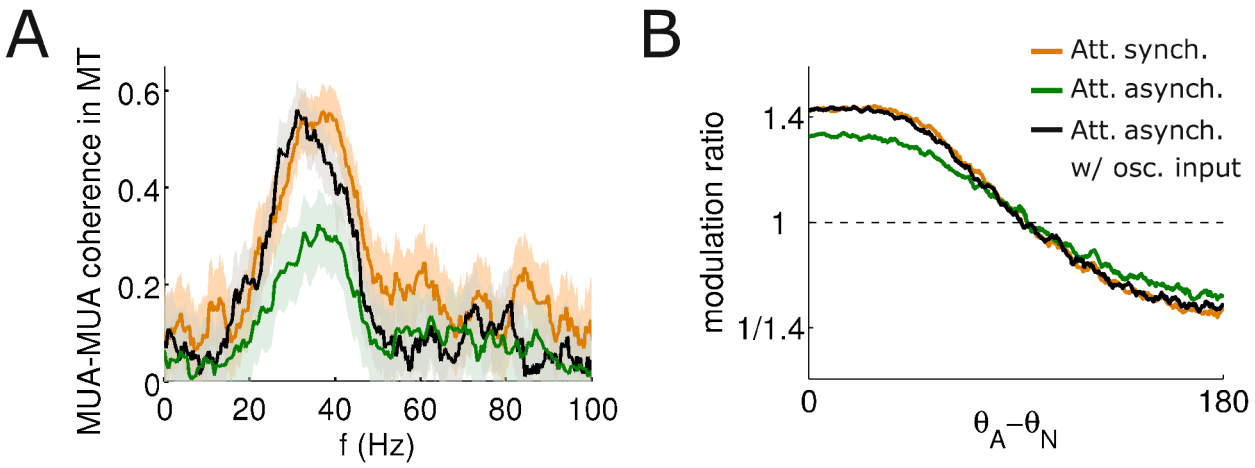

Supplemental Figure 7. Local synchrony enhancement by attention in MT underlies the slight refinement of MT population activity.

A, When the MT network received a zero-mean 35-Hz oscillating input in addition to the PFC top-down with randomly-dispersed long latencies, intra-MT coherence increased (black trace) from the low level caused by random latencies (green trace) to the control level of synchronizing PFC input (orange trace). Notice that, because of the random top-down latencies, the high coherence in the black trace is not concomitant with significant PFC-MT coherence, as for the orange trace. ***B***, Firing rate modulations, relative to the non-attention case, also recovered from the case of random top-down latencies (green trace) to the control case (orange trace). Note that in our model, the PFC module represents a single cortical circuit from which the attentional signal emanates. By this figure's analysis we are not proposing third attentionally-related areas (an increase in model complexity not justified by current data), but to show that: 1) the sources for the two attentional contributions (mean input and synchronization enhancements) may be separated or not, with equal MT attentional effects; 2) attentionally-related inter-areal synchrony, either with PFC or with other cortical areas, is the mechanism underlying the enhancement of local oscillatory activity in area MT in our model; and 3) such local synchrony potentiation is what underpins the slight refinement of the MT activity profile by synchronization in selective attention. Our model integrates these separable contributions of the attentional signal in a generic PFC-MT network, as the most parsimonious model of currently available data.

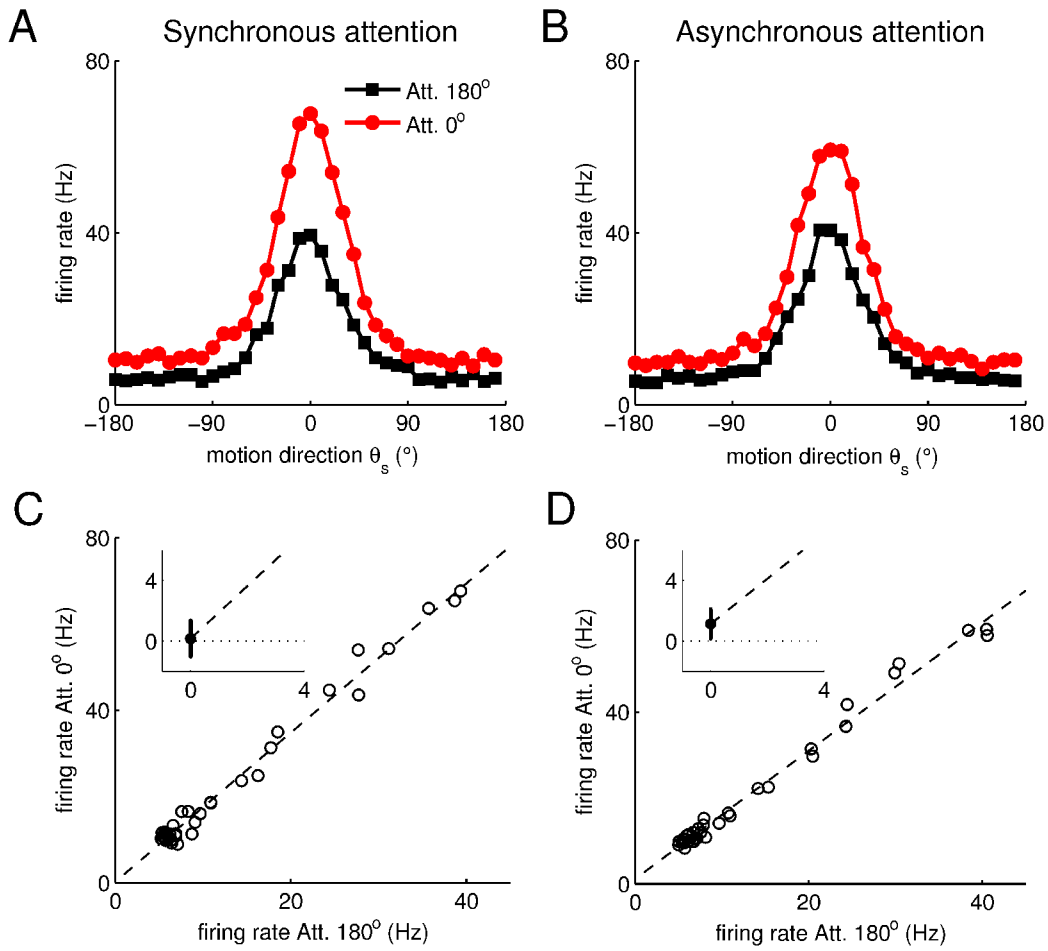

Supplemental Figure 8. Multiplicative gain modulation of responses is potentiated by inter-areal synchrony.

A, Average firing rate of a neuron (preferred direction of motion θ=0º) in trials where the test stimulus direction of motion θ_s was changed continuously from -180º to 180º, and where the attended feature stored in PFC was maintained either at the neuron's preference (0º, red curve), or at the neuron's null direction (180º, black curve). ***B,*** Same for the case when long random synaptic delays were introduced in the top-down attentional signal (Fig. 6). ***C,*** The two curves in ***A*** are very approximately multiplicatively related. This is shown by plotting one against the other, and fitting with a linear regression. The intersect of the regression line with the y-axis includes zero in the 95% confidence interval of the estimation (inset), in agreement with an exact multiplicative relationship between the curves in ***A***. ***D,*** Same analysis for the case of asynchronous top-down in ***B*** shows that the curves follow approximately a gain modulation change, but the regression line does not include zero in the 95% C.I. of its y-axis intersect (inset). Although the difference is small, this proves that inter-areal synchrony improves the multiplicative character of modulatory responses to additive bias inputs.

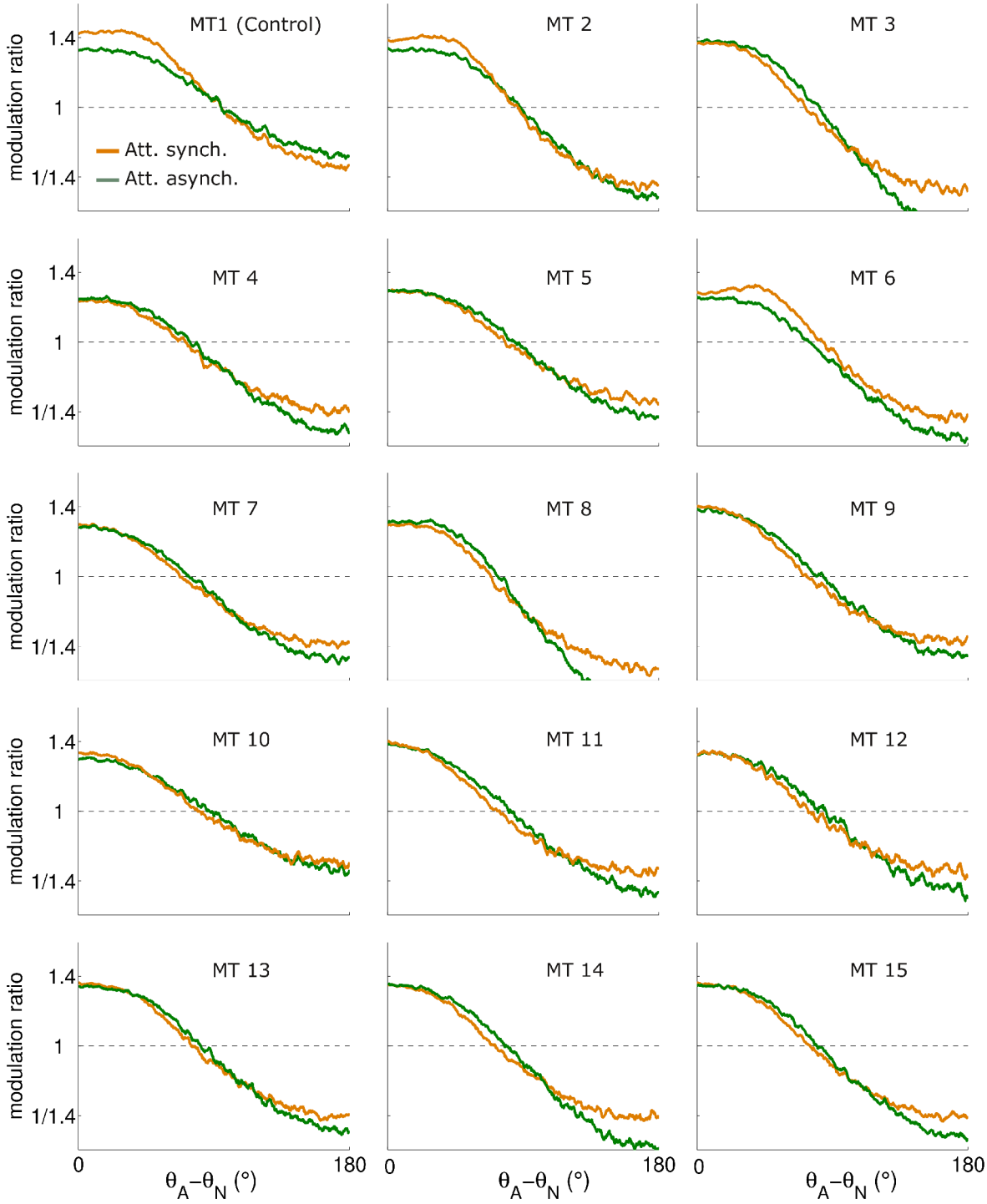

Supplemental Figure 9. None of the MT networks in supplemental Figure 1 showed significant effects of inter-areal synchronization on attentional rate modulations in MT.

Qualitatively different model solutions for area MT (in each panel), found using our optimization procedure (see supplemental Figs. 1, 2, and supplemental Methods), were coupled with the PFC network in order to obtain similar firing rate modulations by attention (orange lines in all panels).

When widely dispersed random latencies were introduced in the top-down input from PFC to MT, the resulting firing rate modulations (green curves) were unaffected or only slightly affected (MT1, MT2 and MT6). This indicates that inter-areal synchronization had weak effects on firing rate encoding in area MT irrespective of the parametric details of the MT network model.

Supplemental Methods

Despite the correspondence with experimental results, many parameters of a theoretical model simulation are not specified experimentally, and constitute the set of free parameters that the modeler tunes in order to simulate a specific brain function. Usually, the approximation to this problem is by manual trial-and-error: trying different sets of parameters with the only help of intuition and experience. This procedure is quite ineffective, as it involves a long, tedious, and often frustrating hand-tuning period. Furthermore, even though a model solution is found, one cannot be sure that qualitatively different model solutions may also exist, or even that the solution found represents a reasonably big portion of the possible models.

Here, we are dealing with correlates of selective attention on the visual motion processing in area MT. We have shown that inter-areal synchronization between the working memory circuit and the sensory module is able to enhance moderately the attentional modulations in the mean rate activity of the MT sensory neurons. Nevertheless, with a single model solution for motion processing in MT we are not in a position to say whether other possible alternative solutions could present much larger impact of inter-areal synchronization on mean rate activity.

To evaluate this aspect we use here a novel approach to tune large neuronal networks, which exploits the power of an optimization algorithm in order to explore much more efficiently the set of free parameters. In this way, we can find different model solutions in an automated, unbiased way. Still, it is not possible to explore the whole infinite hyperspace of parameters, and the answer to our question cannot be final. However, with a number of different model solutions found in an unbiased way, we can certainly acquire an understanding about how robust our result is. In the next sections, we introduce this technique, beginning with a detailed description of the inputs and network parameters in area MT, following with the constraints (*fitness functions*) that we have considered in order to consider a given network an MT model solution. Finally, we describe in detail the optimization method used.

Sensory input to MT. One third of cells in V1 are direction-selective, and they are the main afferent input to MT (Zeki, 1974; Maunsell and Van Essen, 1983; Albright, 1984; Mikami et al., 1986; Born and Bradley, 2005). For simplicity, we have modeled the sensory input from V1 to MT network as a selective injected current (Poisson synaptic inputs were also tested with equivalent results). We modeled this V1 input according to the three main properties of V1 activity for moving random-dot patterns (RDPs): direction-selectivity of these cells (Albright, 1984; Snowden et al., 1992), sensory response saturation in V1 (Snowden et al., 1992), and absence of sensory response

suppression (Snowden et al., 1991; Qian and Andersen, 1994, 1995). Saturation implies that two RDPs moving in the neuron's preferred direction, *separation*=0º, do not suppress, nor enhance neuronal activity. Response suppression may occur when an RDP is moving in the preferred direction and simultaneously another RDP moves in the neuron's null direction, *separation*=180º, as occurs in area MT. However, this is not observed for V1 direction-selective cells: the appearance of another RDP in the neuron's RF moving in whatever direction does not modify the neuron's activity (see supplemental Fig. 1*B*).

The bottom-up input from V1 to MT is totally described by three parameters (supplemental Eq. 1): the baseline (I_0), the amplitude (I_1) and the width of the bell-shaped curve (μ). The selectivity of this input depends on I_1 , I_0 and μ . Thus, for single motion, the bottom-up input is:

$$I_S = I_0 + I_1 \exp\left(\mu\left[\cos(\theta - \theta_C) - 1\right]\right) \qquad \text{(Supplemental Eq. 1)}$$

where θ_C represents the direction of motion of the visual stimulus. On the one hand, this equation agrees with the periodicity of the direction of motion. On the other hand, it is a bell-shaped curve, very similar to a Gaussian curve, where their respective widths are closely related by $\mu \simeq 1/(2\pi\sigma)^2$, being σ the width of the approximating Gaussian curve.

For transparent motion (RDPs in directions θ_{C1} and θ_{C2}), the bottom-up input is:

$$I_S = I_0 + I_1 \frac{\exp\left(\mu\left[\cos(\theta - \theta_{C1}) - 1\right]\right) + \exp\left(\mu\left[\cos(\theta - \theta_{C2}) - 1\right]\right)}{max\left[\exp\left(\mu\left[\cos(\theta - \theta_{C1}) - 1\right]\right) + \exp\left(\mu\left[\cos(\theta - \theta_{C2}) - 1\right]\right)\right]} \qquad \text{(Supplemental Eq. 2)}$$

and it fulfills both the saturation and lack of suppression properties, as the maximal input is $I_0 + I_1$ independently of how many RDPs are presented and independently of the separation between θ_{C1} and θ_{C2}.

Parameters in the MT model simulation. The MT network model has $N = 40$ different parameters that describe completely its behavior. From them, $N' = 16$ are well-characterized electrophysiologically. These are the intrinsic parameters that describe E-cells and I-cells in the integrate-and-fire formalism: membrane capacitance (C_m), leak conductance and reversal potential (g_L , E_L), firing threshold and reset potentials (V_{th} , V_r) and refractory time (τ_{ref}). We also have good estimation for parameters defining the dynamics of conductance-based synapses (τ_{AMPA} , $\tau_{s,NMDA}$, $\tau_{x,NMDA}$, $\alpha_{s,NMDA}$, τ_{GABA_A}) and their synaptic reversal potentials (V_E , V_I).

As the number of remaining free parameters is very high ($N - N' = 24$), the hyperspace of

parameters that remains is still too big to be considered in its completeness. In order to reduce it, we used our experience and intuition with these network simulations to choose $n=13$ free parameters that will be explored using the optimization algorithm for the MT network model. The chosen parameters refer to: the sensory input from V1 to MT (input strengths to each cell population: I_0^E, I_1^E, I_0^I, I_1^I, and the width μ, which we assume equal for the two populations); the strength of local conductances ($G_{EE,AMPA}$, $G_{EE,NMDA}$, $G_{EI,AMPA}$, $G_{EI,NMDA}$, G_{IE}, G_{II}); and the maximum external Poisson synaptic conductances ($g_{ext,E}$, $g_{ext,I}$). The remaining parameters (number of neurons in each population, selectivity in recurrent connectivities, and rate of the uncorrelated Poisson spike trains in each neuron) remain fixed during the whole execution.

Fitness functions. The space of all possible set of free parameters is named $SP \subseteq \Re^n$, where *n* denotes the number of free parameters, $n=13$ in our case, as it has been explained above. To evaluate the goodness of a set of parameters $P \in SP$, it is necessary to run three kinds of simulations (7 simulations in total): one simulation without visual stimulation (spontaneous activity), one simulation with a single moving RDP, and five simulations with two RDPs in transparent motion and varying separation between the directions of motion of each component: 30°, 60°, 90°, 120° and 180°, respectively. A "good" set of parameters *P* must mimic real behavior, as extracted from experimental results:

- We put restrictions in the values of the mean spontaneous activity to be in agreement with the experimental observations (Maunsell and Van Essen, 1983; Mikami et al., 1986). Thus, we require spontaneous activity to lie within the interval [7, 11] Hz for E-cells.
- We consider the activity of E-cells in MT when an RDP is moving coherently in their receptive field (RF). It has been found that preferred directions of motion present strong enhancements in the neural responses but non-preferred directions generate in average slight suppressions (Britten et al., 1993; Britten and Newsome, 1998). Then, we require the maximum activity for E-cells during single moving RDP to be within the range [38, 47] Hz, and the minimum activity to be slightly smaller (by 0.5-2.5 Hz) than the spontaneous activity.
- We constrain the model not to have too high inhibitory activity: the mean spontaneous activity without stimulation and the minimum activity during single moving RDP must be below 30 Hz, and the maximum activity during single moving RDP must be below 60 Hz for I-cells in the model.

- Finally, we want to include the observed MT activity normalization for E-cells (Snowden et al., 1992; Qian and Andersen, 1994, 1995; Simoncelli and Heeger, 1998; Treue et al., 2000): the average activity in the population is conserved for RDPs in transparent motion with respect to a single moving RDP, and that occurs independently of the separation between the two components of motion (with a tolerance of 5% in the model).

Since there is high variability in the neural activity, we average steady-state responses in a window of 5 s simulation. After defining the previous list of conditions, that we expect an MT network model solution to satisfy, we developed statistical and heuristic measures that evaluate automatically the goodness of simulation results, given a set of parameters $P \in SP$. Specifically, the steps to follow for the evaluation are:

- A fitness function is designed according to each condition in the previous list.
- All the fitness functions are calculated for the given set of parameters $P \in SP$.
- Each fitness function is weighted by a specific multiplicative factor (the values that these weights take are important to be able to find a solution to the problem, also the speed of convergence of the algorithm strongly depends on them).
- Finally, the fitness value $Fit(P)$, to a given set of parameters $P \in SP$, is computed as the sum of all the weighted fitness functions.

Searching algorithm. As described in (Kennedy and Eberhart, 1995, 2001), the Particle Swarm Optimization algorithm (PSO) is an adaptive algorithm based on a social environment where a set of particles, called population, are visiting different "positions" of a given domain. In our context, this domain is a bounded region of the space of free parameters SP, where we anticipate solutions for our network to exist. Each possible particle in SP therefore specifies all the parameters for a network simulation, which can then be run in the computer and a fitness value can be computed (see the previous sections above). PSO is designed to search among SP the best evaluated sets. At each iteration particles will move (i.e. new parameters will be chosen from SP) returning stochastically toward the population's best fitness position (social knowledge) and the particle's own previous best fitness position (cognitive knowledge or self-knowledge). Particles of the population share information of the best areas to search.

Let us denote PAR the set of n parameters and let PO be the population of particles. At each iteration, x_{fp} and v_{fp} denote respectively the current value and the current velocity of the

parameter $p \in PAR$ for the particle $f \in PO$. Then, $\vec{x_f} = \{x_{fp}\}_{p=1..n}$ and $\vec{v_f} = \{v_{fp}\}_{p=1..n}$ are the vectors of the current position and the current velocity of particle f. The movements of the particles are defined by the following equations (see supplemental Fig. 1*A*):

$$v_{fp}(i+1) = w\, v_{fp}(i) + r_1 c_1 (x_{fp}(i) - b_{lfp}) + r_2 c_2 (x_{fp}(i) - b_{gp}) \qquad \text{(Supplemental Eq. 3)}$$

$$x_{fp}(i+1) = x_{fp}(i) + \chi\, v_{fp} \qquad \text{(Supplemental Eq. 4)}$$

where c_1, c_2 are integer non-negative values, named cognitive and social values respectively (they are equal to 2 in our implementation). r_1, r_2 are real values drawn randomly from [0, 1], w and χ are non-negative real values, named respectively inertia weight and constriction factor (their values are respectively 0.729 and 0.95^k, where k is the iteration number), b_{gp} is the value of parameter p pertaining to the best set of parameters found by the population (social knowledge) and b_{lfp} is the value of parameter p pertaining to the best parameters set found by particle f (self-knowledge). In supplemental Eq. 3, the first term refers to the previous velocity (inertia term), and the second and the third terms are related respectively to the distance to the best set of parameters found by the particle (cognitive knowledge) and to the distance to the best set of parameters found by the population (social knowledge). We have chosen PSO as a searching algorithm because it is able to work on any fitness function and it is easy to implement on real parameters. PSO has been efficiently used as an optimizing method for a variety of problems (Kennedy and Eberhart, 2001), although to our knowledge this is the first time it is used in Neuroscience.

Technical implementation. In our experiment, particle positions are each set of parameter values $P \in SP$ that define an MT network model. Particles are initially randomly instantiated to a position within the allowed hyperspace and simulations are run for each particle. After running 7 simulations per particle, fitness functions are computed for each particle. Following PSO, particles are moved and new positions are assigned to each particle. PSO and fitness functions are computationally affordable but simulations are computationally very expensive and many need to be run to perform one single evaluation. Each simulation lasts in average 20-50 minutes. For each position visited, 7 simulations are run, that gives ~4 hours. A swarm with 50 particles would need ~200 hours at each movement phase. If each experiment lasts ~50 iterations, then ~10,000 hours of CPU processing time are necessary per experiment. We ran these intensive simulations in large clusters of computers (including MareNostrum Supercomputer at the *Barcelona Supercomputing Center*). These

simulations involve three separate codes:

- the worker code: the biological neural network simulation of the MT cortical microcircuit.
- the master code: a code to control the simulation that, at each time step, evaluates the behavior of the population of neural network simulations, updates the parameters to advance towards the required optimization following the PSO algorithm, and launches the new simulations.
- the Grid SuperScalar application (Sirvent et al., 2006), that allows an easy granular parallelization of the previous two items.

Thus, our approach consists in processing, at each iteration, a myriad of small jobs (the biological neural network simulation for area MT, which we call the worker code). Each job is completed within a single computational node, under the control and evaluation of the master code that implements the optimization algorithm (PSO). The Grid SuperScalar technology provided the right computational tool to deploy this efficiently in a large cluster of computers (Sirvent et al., 2006).

Representative MT model solution. In this section we present a characteristic network model solution for visual motion processing in area MT (supplemental Fig. 1*C*), derived by using the PSO algorithm described in the previous sections. The unspecific Poisson external input is responsible of the neurons' spontaneous activity, generating a firing rate for the chosen solution close to 10 Hz. The MT network model shows both the direction selectivity and the population activity normalization found in area MT (supplemental Fig. 1*C*). This kind of normalization implies that increasing the separation in terms of the direction of motion between two transparent RDPs generates a reduction in the activity of the neurons that code for them (Treue et al., 2000). Moreover, the same experimental observations show that the averaged response in MT for transparent RDPs is well-fitted by the sum of two Gaussian curves divided by 2, trend that our model solutions reproduce quite approximately, too (with a 5% tolerance). This kind of fit maintains constant the area under the curve independently of the RDPs separation, showing that the average activity for the population profile is conserved, even when the peak activity decreases with such separation. Such kind of population normalization was already used in another MT model, although it was imposed without considering plausible physiological mechanisms (Simoncelli and Heeger, 1998). The PSO algorithm found 15 different biophysically plausible network models for area MT (supplemental Fig. 2). In order to generate the population normalization, we show here that the main characteristic of the MT network model is that the circuit is dominated by inhibition: recurrent

inhibition in the model is much higher than recurrent excitation for all MT network model solutions.

References

Albright TD (1984) Direction and orientation selectivity of neurons in visual area MT of the macaque. J Neurophysiol 52:1106-1130

Ardid S, Wang X-J, Compte A (2007) An integrated microcircuit model of attentional processing in the neocortex. J Neurosci 27:8486-95

Born RT, Bradley DC (2005) Structure and function of visual area MT. Annu Rev Neurosci 28:157-189

Britten KH, Newsome WT (1998) Tuning bandwidths for near-threshold stimuli in area MT. J Neurophysiol 80:762-770

Britten KH, Shadlen MN, Newsome WT, Movshon JA (1993) Responses of neurons in macaque MT to stochastic motion signals. Vis Neurosci 10:1157-69

Fanardjian VV, Papoyan EV (1997) Patterns of inputs to the parietal cortex efferent neurons from the motor cortex and cerebellum in the cat. Neuroscience 77:965-74

Ghosh S, Porter R (1988) Corticocortical synaptic influences on morphologically identified pyramidal neurones in the motor cortex of the monkey. J Physiol 400:617-29

Kennedy J, Eberhart R (1995) Particle swarm optimization. In: Proceedings of the IEEE International Conference on Neural Networks , pp. 1942-1948 vol.4.

Kennedy J, Eberhart RC (2001) Swarm Intelligence. Morgan Kaufmann Publishers Inc.

Le Bé J, Silberberg G, Wang Y, Markram H (2007) Morphological, electrophysiological, and synaptic properties of corticocallosal pyramidal cells in the neonatal rat neocortex. Cereb Cortex 17:2204-13

Maunsell JH, Van Essen DC (1983) Functional properties of neurons in middle temporal visual area of the macaque monkey. I. Selectivity for stimulus direction, speed, and orientation. J Neurophysiol 49:1127-1147

Mikami A, Newsome WT, Wurtz RH (1986) Motion selectivity in macaque visual cortex. II. Spatiotemporal range of directional interactions in MT and V1. J Neurophysiol 55:1328-1339

Qian N, Andersen R (1994) Transparent motion perception as detection of unbalanced motion signals. II. Physiology. J Neurosci 14:7367-7380

Qian N, Andersen RA (1995) VI responses to transparent and nontransparent motions. Exp Brain Res 103:41-50

Simoncelli EP, Heeger DJ (1998) A model of neuronal responses in visual area MT. Vision Res 38:743-761

Sirota MG, Swadlow HA, Beloozerova IN (2005) Three channels of corticothalamic communication during locomotion. J Neurosci 25:5915-5925

Sirvent R, Pérez JM, Badia RM, Labarta J (2006) Automatic Grid workflow based on imperative programming languages. Concurrency Computat Pract Exper 18:1169-1186

Snowden RJ, Treue S, Andersen RA (1992) The response of neurons in areas V1 and MT of the alert rhesus monkey to moving random dot patterns. Exp Brain Res 88:389-400

Snowden RJ, Treue S, Erickson RG, Andersen RA (1991) The response of area MT and V1 neurons to transparent motion. J Neurosci 11:2768-2785

Treue S, Hol K, Rauber HJ (2000) Seeing multiple directions of motion-physiology and psychophysics. Nat Neurosci 3:270-276

Zeki SM (1974) Functional organization of a visual area in the posterior bank of the superior temporal sulcus of the rhesus monkey. J Physiol 236:549-573

Supplemental Table

	μ	I_0^E (nA)	I_1^E (nA)	I_0^I (nA)	I_1^I (nA)	$G_{EE,AMPA}$ (nS)	$G_{EE,NMDA}$ (nS)	$G_{EI,AMPA}$ (nS)	$G_{EI,NMDA}$ (nS)	G_{IE} (nS)	G_{II} (nS)	$g_{ext,E}$ (nS)	$g_{ext,I}$ (nS)
$MT_{1\ (Control)}$	2.63	1.65	0.740	1.40	0.390	0.801	1.10	0.684	2.00	7.34	7.34	17.0	9.20
MT_2	2.53	1.00	0.900	0.200	0.180	4.88E-3	0.0927	4.88E-3	0.195	1.46	0.391	15.0	4.50
MT_3	1.51	1.45	2.06	0.372	0.691	0.694	0.469	1.81	0.948	7.70	6.18	29.5	16.6
MT_4	2.08	1.73	1.47	1.28	0.768	0.271	0.0246	1.48	0.679	7.80	7.72	19.4	9.51
MT_5	2.95	1.86	1.11	0.414	0.141	0.378	0.144	1.19	0.0891	6.73	2.28	17.5	3.28
MT_6	2.53	1.00	0.900	0.200	0.180	0.269	0.00	0.0488	0.195	1.46	0.391	15.0	4.50
MT_7	3.04	2.61	1.08	0.684	0.192	0.635	1.23	1.39	1.31	7.48	4.53	23.9	8.02
MT_8	1.93	2.41	0.880	1.19	0.465	0.934	1.21	1.61	0.778	7.66	5.74	22.0	15.5
MT_9	2.99	1.89	0.861	1.45	0.443	0.236	0.465	1.69	0.757	7.31	7.50	13.5	5.91
MT_{10}	2.67	1.59	1.30	0.526	0.319	1.40	0.752	1.73	1.28	7.72	5.34	25.9	10.6
MT_{11}	1.57	2.62	1.99	1.44	0.295	0.969	0.168	1.89	1.82	7.44	6.93	29.4	12.3
MT_{12}	1.26	3.28	1.44	1.09	0.329	1.25	0.589	1.37	1.02	7.56	4.83	25.7	10.7
MT_{13}	1.71	2.86	1.48	0.646	0.411	0.592	0.0345	1.81	0.786	6.36	5.53	25.7	12.6
MT_{14}	2.63	1.65	0.829	1.40	0.392	0.724	1.14	1.34	1.78	7.36	7.34	16.9	9.18
MT_{15}	2.08	2.45	1.60	0.0241	0.202	0.0202	0.145	0.855	1.00	6.58	3.37	26.5	4.69
Mean	2.27	2.00	1.24	0.821	0.360	0.612	0.505	1.26	0.976	6.53	5.03	21.5	9.13
SD	0.581	0.671	0.421	0.519	0.183	0.419	0.472	0.607	0.588	2.10	2.44	5.49	4.06
% SD/Mean	25.5	33.5	33.9	63.3	51.0	68.6	93.4	48.2	60.2	32.2	48.6	25.5	44.5

Supplemental Table 1. Subset of free parameters considered in our optimization procedure and their specific values in each MT network model solution.

Basic statistics for each parameter between models are indicated in the three bottom rows (mean, standard deviation and coefficient of variation, i.e. standard deviation relative to the mean), to stress the variance of the different MT model solutions in the space of parameters. Notice that for any parameter the standard deviation relative to the mean is >25%, and in more than half of the parameters it is higher or very close to 50%.